European Journal of Mechanics B/Fluids 47 (2014) 145–150

Contents lists available at ScienceDirect

European Journal of Mechanics B/Fluids

journal homepage: www.elsevier.com/locate/ejmflu

Cloaking a circular cylinder in water waves

J.N. Newman

Department of Mechanical Engineering (Emeritus), MIT, Cambridge, MA 02139, USA

ARTICLE INFO

Article history:
Available online 22 November 2013

Keywords:
Linear water-wave theory
Diffraction
Cloaking

ABSTRACT

In the diffraction of water waves by fixed bodies, the scattered waves propagate outward in the far field and attenuate with increasing distance from the structure. 'Cloaking' refers to the reduction in amplitude or complete elimination of the scattered waves. The possibility of cloaking is of both scientific and practical interests.

Cloaking is considered here for a circular cylinder on the free surface, surrounded by one or more additional bodies. Linearized time-harmonic motion is assumed. A numerical procedure is used to optimize the geometry of the surrounding bodies, so as to minimize the energy of the scattered waves. Values of the scattered energy are achieved which are practically zero at a specific wavenumber, within the estimated numerical accuracy. This provides tentative support for the existence of perfect cloaking, and conclusive evidence that structures can be designed to have very small values of the mean drift force.

Dedicated to the memory of Enok Palm, an inspiring colleague and friend

1. Introduction

In the three-dimensional diffraction problem, where plane waves are incident upon a fixed structure, scattered waves generally exist in the far field. The word 'cloaking' is used in various fields of wave motion to refer to the reduction in amplitude or complete elimination of the scattered waves. This is achieved by modifying the shape of the structure or the properties of the surrounding medium. 'Perfect cloaking' refers to the condition where there are no scattered waves in any direction. The possibility of perfect cloaking in the diffraction of water waves is of scientific interest, since it is not known if this condition can be achieved with a structure of non-zero volume on or near the free surface.

Cloaking may also have practical applications in the design of offshore structures, particularly with respect to the mean drift force. When scattering occurs the time-averaged second-order pressure exerts a steady drift force on the structure, in the direction of propagation of the incident waves. This drift force can be related by momentum conservation to the amplitude of the scattered waves. Thus the mean drift force is zero if there are no scattered waves.

Energy is transported by the scattered waves as they propagate outward on the free surface. The total scattered energy is defined here as the integral of the rate of energy flux across a control surface surrounding the structure. In an ideal fluid the mean rate of energy flux is constant, independent of the control surface. Since the energy is proportional to the square of the wave amplitude it follows that the amplitude is proportional to the inverse square-root of the radius. If there are no scattered waves the scattered energy is equal to zero. Thus the scattered energy is an appropriate measure of cloaking, analogous to the scattering cross-section in other fields.

Cloaking a bottom-mounted circular cylinder has been considered by Porter and Newman [1–3], using an annular bed with a variable depth to refract the waves around the cylinder. Their computations show that near-zero values of the scattered energy can be achieved by optimizing the bathymetry of the bed. However the use of variable bathymetry may be impractical, especially in deep water. Thus the present work considers the possibility of cloaking a circular cylinder which is fixed on the free surface in a fluid of infinite depth, by surrounding it with one or more outer bodies. The dimensions of the inner cylinder are fixed, and the scattered energy is minimized at a value of the frequency where the product of the wavenumber and the cylinder draft is equal to one. Linearized time-harmonic motion of an ideal fluid is assumed.

Two specific types of surrounding structures are used to cloak the inner cylinder. The first is an array of outer cylinders which surround the inner cylinder, as shown in Fig. 1. This configuration was suggested by the work of Farhat et al. [4], who showed that a large number of small circular cylinders could be used to cloak an inner cylinder in problems governed by the two-dimensional wave equation. The second type is a continuous 'ring', such as a torus with constant cross-section or a non-axisymmetric body with varying cross-section. This type was suggested by the results for the arrays of cylinders, where the scattered energy is reduced progressively by increasing the number of cylinders and decreasing

E-mail address: jnn@mit.edu.

0997-7546/$ – see front matter
http://dx.doi.org/10.1016/j.euromechflu.2013.11.005

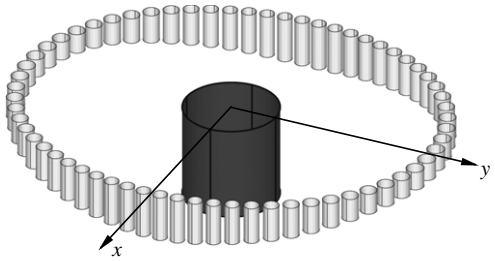

Fig. 1. Perspective view of the structure with $M = 64$ outer cylinders and $N = 15$ optimization parameters. Only the submerged surfaces are shown, with the upper edge of each cylinder in the plane $z = 0$.

their spacing. For both types it is shown that the scattered energy can be reduced to very small values by optimizing the dimensions and shape of the surrounding structure.

The structures are assumed to be symmetric about the planes $x = 0$ and $y = 0$, where the x-axis is in the direction of incident-wave propagation. Symmetry about $x = 0$ is suggested by reversing time (or conjugating the solution of the boundary-value problem with complex time-dependence). Thus, for any structure with no scattered waves, there also are no scattered waves if the incident-wave direction is reversed. This implies that the structure itself should be symmetric about $x = 0$. Symmetry about $y = 0$ is more obvious, since the incident-wave field is independent of y.

Preliminary results, which are more limited and less accurate, have been presented in [5]. The possibility of perfect cloaking with an axisymmetric structure was considered there. The results in [5] suggest that this might be possible, although it would be remarkable if perfect cloaking could be achieved with such a structure. The results presented here, which are more accurate, suggest that perfect cloaking can only be achieved with non-axisymmetric structures.

The theory and computational method are described in Sections 2 and 3. Results for the two types of surrounding structures are presented in Sections 4 and 5. These results are compared and discussed in Section 6.

2. Theory

A fixed structure consisting of two or more rigid bodies is situated on the free surface of the fluid, which is inviscid, incompressible, and extends to infinity in all horizontal directions. The fluid depth is infinite. Cartesian coordinates $\mathbf{x} = (x, y, z)$ are used with $z = 0$ the plane of the undisturbed free surface and z positive upward. Harmonic time-dependence is assumed, with the velocity potential

$$\Phi(\mathbf{x}, t) = \mathrm{Re}\left\{\phi(\mathbf{x})\mathrm{e}^{\mathrm{i}\omega t}\right\}. \tag{1}$$

Here t represents time, ω is the radian frequency, and ϕ is complex. The potential is a solution of the Laplace equation

$$\nabla^2\phi = 0 \tag{2}$$

in the fluid domain. Small amplitude motions are assumed, justifying the linearized free-surface boundary condition

$$K\phi - \phi_z = 0 \quad \text{on } z = 0, \tag{3}$$

where $K = \omega^2/g$ is the wavenumber and g is the gravitational acceleration. Subscripted lower-case letters denote partial differentiation. Since the fluid velocity vanishes at large depths,

$$\nabla\phi \to 0 \quad \text{as } z \to -\infty. \tag{4}$$

In the diffraction problem the structure is fixed, with plane progressive waves of amplitude A incident upon it. The Neumann boundary condition

$$\phi_n = 0 \tag{5}$$

is applied on the submerged surface S of the structure. The subscript n denotes the normal derivative, with $\mathbf{n}$ positive in the direction out of the fluid domain. The potential is defined in the form

$$\phi = A(\phi_I + \phi_S) \tag{6}$$

where ϕ_I is the incident-wave potential and ϕ_S is the scattering potential, both for unit amplitude A. Without loss of generality it can be assumed that the incident waves propagate in the positive x direction, and thus

$$\phi_I = \frac{g}{\omega}\,\mathrm{e}^{Kz - \mathrm{i}Kx}. \tag{7}$$

The boundary-value problem is completed by imposing the radiation condition in the far-field, which can be expressed in the form

$$\phi_S \simeq \frac{g}{\omega}\,\frac{H(\theta)}{\sqrt{2\pi KR}}\,\mathrm{e}^{Kz - \mathrm{i}KR - \mathrm{i}\pi/4} \quad \text{as } R \to \infty. \tag{8}$$

Here (R, θ) are polar coordinates with $x + \mathrm{i}y = R\mathrm{e}^{\mathrm{i}\theta}$. The function $H(\theta)$, which represents the amplitude of the scattered waves, is known as the Kochin function. Following the analysis in [6], the Kochin function can be evaluated by applying Green's theorem, with the result

$$H(\theta) = \frac{\omega K}{g}\iint_S \left(\phi_{Sn} - \phi_S\frac{\partial}{\partial n}\right)\mathrm{e}^{Kz + \mathrm{i}K(x\cos\theta + y\sin\theta)}\,dS. \tag{9}$$

The normalized rate of scattered energy is given by the dual relations

$$E = \frac{1}{2\pi}\int_0^{2\pi} |H(\theta)|^2 d\theta = -2\mathrm{Im}\left\{H(0)\right\}. \tag{10}$$

The equivalence of these two relations follows from Green's theorem, as shown in [6], or more physically from the conservation of energy applied to the total potential (6). In other types of wave diffraction this equivalence is known as the optical theorem.

If the structure is symmetric about $x = 0$, the symmetric and anti-symmetric components of the potential ϕ_S satisfy Neumann boundary conditions on the body where the normal derivatives are real and imaginary, respectively. If there is no scattered energy these potentials vanish at infinity faster than a radiated wave, and satisfy the homogeneous boundary condition (3) on the free surface. It follows that the symmetric and anti-symmetric components of the potential are respectively real and imaginary throughout the fluid domain, assuming uniqueness. This property has important effects on the mean second-order pressure and drift force, as will be noted below.

3. Computational method

Our objective is to surround a prescribed inner body with one or more outer bodies which are optimized to minimize the scattered energy of the combined structure. The inner body is a circular cylinder with radius 0.5 m and draft 1.0 m. The optimization is performed at the wavenumber $K = 1$, using non-dimensional parameters normalized by the unit draft. The energy E is normalized by the corresponding value for the uncloaked cylinder, $E_0 = 0.0727344$. The energy ratio E/E_0 is defined in this manner.

The computational approach combines a three-dimensional radiation–diffraction code based on the boundary-integral-equation method (BIEM) with a multi-variate optimization code (PRAXIS).

The BIEM code, a modified version of the program WAMIT [7], evaluates the scattered energy for a structure with specified geometry which is defined parametrically. PRAXIS, which is described in [8], searches for optimum values of the geometric parameters such that the scattered energy is minimized.

In the BIEM the unknown potential is the solution of an integral equation over the boundary surface of the fluid domain, based on Green's theorem. The free-surface Green function is used to reduce the computational domain to the body surface (the submerged surface of the structure). The geometry of the body surface is mapped analytically to a set of square domains in a two-dimensional parametric space, and the potential is represented in these domains by continuous B-splines. A Galerkin method is used to reduce the integral equation to a linear system, which is solved by Gaussian elimination. Further details are given in [7,9]. The scattered energy E is evaluated using the two alternative values in (10), and the maximum of these two values is used as the objective function.

PRAXIS iterates to find optimum values of the geometric parameters which minimize the objective function. Typically a large number of iterations is required, on the order of 1000 for the results presented here. In many cases it is necessary to re-start the optimization with modified initial values of the parameters, to avoid false convergence.

In the simplest cases presented here there are three geometric parameters. For the array of circular cylinders these include their radius r, draft d, and the radius R_0 of their axes from the center of the inner cylinder, if these parameters are the same for all of the outer cylinders. For the torus the corresponding parameters are the major and minor semi-axes of the elliptical cross-section and the radius. For more general geometries the number of parameters N is increased. As expected, the minimum value of E is reduced by increasing N.

The principal restrictions on the computational accuracy are in the BIEM, due to the discretization used in the Galerkin method and in the integration of the solution over the body surface, and also due to the evaluation of the free-surface Green function and its derivatives. The discretization accuracy is controlled by increasing the panel subdivisions in the parametric space, and judging the accuracy of the results from convergence tests. The accuracy of the numerical integrations is controlled by increasing the number of panels, and by using adaptive quadratures for the Rankine (singular) part of the Green function. The accuracy of the Green functions depends on the algorithms used for their evaluations, as discussed below.

The results presented in [5] were obtained using a single-precision BIEM code which was adapted from the standard version of WAMIT [7]. The absolute accuracy of the hydrodynamic parameters including the scattered energy is estimated to be between 3 and 5 decimals. The minimum values of E/E_0 achieved with this code are on the order of 10^{-4}. From the viewpoint of practical engineering applications these values are effectively zero, but for the scientific objective of establishing the existence of perfect cloaking they are too large to be conclusive.

In order to extend the accuracy of the present work a double-precision BIEM program has been developed from WAMIT. A special subroutine is used to evaluate the free-surface Green function and its derivatives, based on the integral representations and expansions in [10]. This achieves absolute accuracies of approximately 12D (decimals) for the Green function and 11D for its first derivatives. Test computations have been made for the added mass and damping of a floating hemisphere. For zero- and infinite-frequencies, where the surge and heave added-mass coefficients are equal to half of the displaced fluid mass, the results are correct to about 12D. Convergence tests at the wavenumber $K = 1$ indicate that the accuracy of the added mass and damping is between 9D and 11D. Similar accuracy is suggested by comparison of the two alternative equations (10) for the scattered energy. The results presented below are consistent with these estimates, with minimum values of the energy ratio E/E_0 of order 10^{-8}.

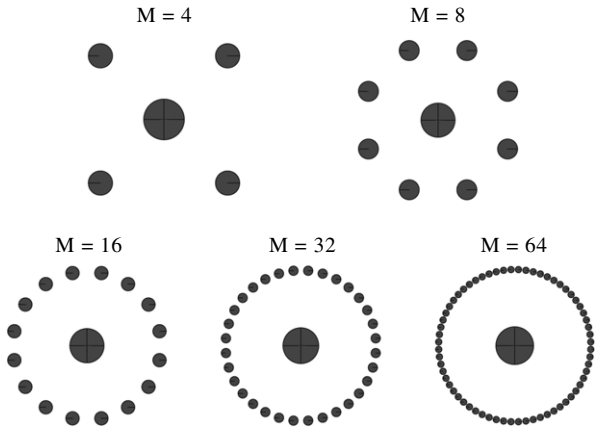

Fig. 2. Plan view of the structures with $M = 4, 8, 16, 32, 64$ outer cylinders and $N = 3$ optimization parameters as shown in Table 1. The incident waves propagate in the x-direction, which is horizontal in the above figures.

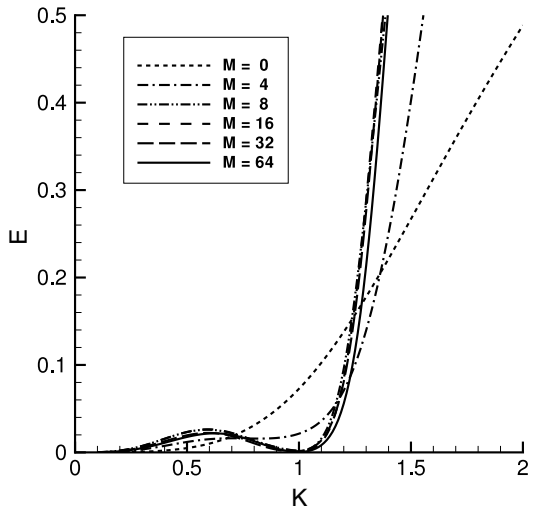

Fig. 3. Scattered energy for the uncloaked cylinder ($M = 0$) and the five optimized structures shown in Fig. 2.

4. Arrays of circular cylinders

In this section we consider structures where the inner cylinder is surrounded by an array of M outer cylinders. In the most general case each outer cylinder has a radius r_m and draft d_m, with its vertical axis at (R_m, θ_m), where $(m = 1, 2, \ldots, M)$. The entire structure is fixed on the free surface. Five different arrays are considered with $M = (4, 8, 16, 32, 64)$. Optimum values of the parameters $(r_m, d_m, R_m, \theta_m)$ are computed to minimize the energy. Since the structures are assumed to be symmetric about $x = 0$ and $y = 0$ the maximum number of independent parameters is $N = M$.

First we consider the simplest case where the parameters $r_m = r$, $d_m = d$ are the same for all of the cylinders, which are uniformly spaced around a circle of radius R_0 as shown in Fig. 2. In this case there are $N = 3$ optimization parameters. The results are summarized in Table 1. The scattered energy ratio decreases as the number of cylinders M is increased. The minimum value obtained

Table 1
Optimized parameters of the arrays where the outer cylinders all have the same dimensions, with uniform spacing ($N = 3$).

M	r	d	R_0	E	E/E_0
4	0.2989	0.5857	2.2091	0.0214	0.2938
8	0.2934	0.6888	2.2032	0.0018	0.0252
16	0.1963	0.6920	2.1579	0.0014	0.0196
32	0.1309	0.6715	2.0991	0.0009	0.0125
64	0.0847	0.6007	2.0128	0.0005	0.0066

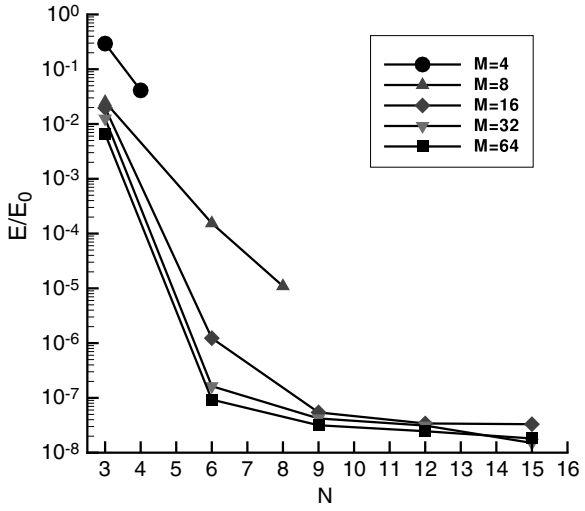

Fig. 4. Scattered energy ratios of the structures with $M = 4, 8, 16, 32, 64$ outer cylinders. N is the number of optimization parameters.

is $E/E_0 = 0.0066$ for $M = 64$. Fig. 3 shows the scattered energy E for a range of wavenumbers. The results for $N \geq 8$ are practically the same, with very small values at $K = 1$ and less energy in the interval $0.7 < K < 1.2$ compared to the uncloaked inner cylinder. Thus broadband cloaking is achieved, within this range of wavenumbers.

More general configurations follow by considering different values of the optimization parameters for each cylinder, defined by the Fourier series

$$\begin{pmatrix} r_m \\ d_m \\ R_m \end{pmatrix} = \sum_{j=1}^{J} \begin{pmatrix} a_{jm} \\ b_{jm} \\ c_{jm} \end{pmatrix} \cos 2(j-1)\theta_m \quad (m = 1, 2, \ldots, M/4). \quad (11)$$

Except as noted below, the angles θ_m are uniformly spaced around a circle, with

$$\theta_m = \frac{\pi}{M}(2m - 1).$$

The number of optimization parameters is $N = 3J$, where $J \leq M/4$.

Fig. 4 shows the optimized energy ratio for different values of M and N. The scattered energy is reduced substantially by varying the parameters for each cylinder; adding only the Fourier term $j = 2$ in (11) reduces E/E_0 to between 10^{-4} and 10^{-7}, depending on the number of cylinders. For the array with 64 cylinders and 15 optimization parameters, $E/E_0 = 1.8 \times 10^{-8}$. A perspective view of this structure is shown in Fig. 1. (The energy ratio for $M = 32$, $N = 15$ is smaller, with the value $E/E_0 = 1.5 \times 10^{-8}$, but this is considered to be an anomaly due to the limits of the numerical accuracy.)

Fig. 5 shows the variation of the parameters (r_m, d_m, R_m) around one quadrant of the array, for the best configurations with different numbers of cylinders. The most significant variation is for the depth d, which is relatively large at the up-wave and down-wave ends of the array and small on the sides, as shown in Fig. 1.

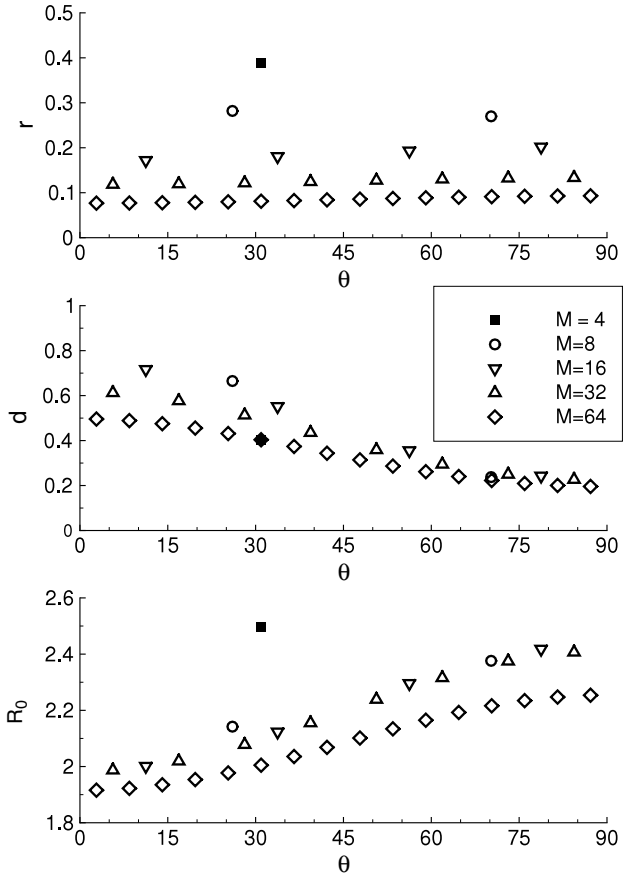

Fig. 5. Azimuthal variation of the cylinder dimensions r, d, R_0. The symbols indicate the angular position of the cylinders in each array. The number of optimization parameters is the maximum for each array shown in Fig. 4. Note that the scale is different in each figure.

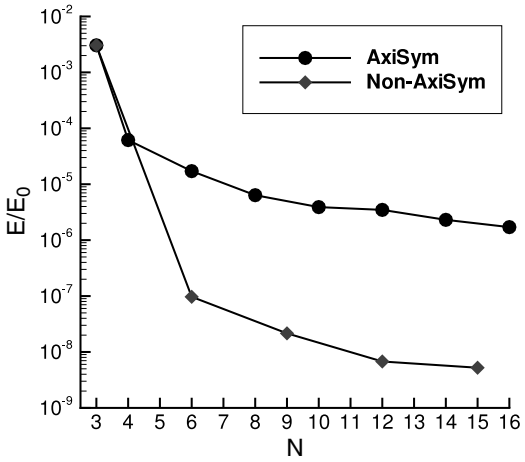

Fig. 6. Scattered energy ratios of the structures with axisymmetric and non-axisymmetric rings. N is the number of optimization parameters. For $N = 3$ both types of ring reduce to a torus with semi-elliptical sections.

One additional generalization which can be included is nonuniform azimuthal spacing between the outer cylinders. If the angles θ_m are defined by Fourier series analogous to (11), $N = 4J$. The only cases where this is relatively advantageous are for 4 and 8 cylinders, as shown in Fig. 4.

Similar results have been obtained from limited computations with other types of bodies, and for a fluid of finite depth.

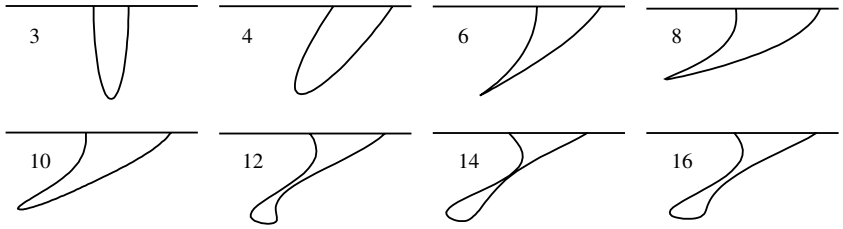

Fig. 7. Cross-sections of the axisymmetric rings. The number of optimization parameters N is shown for each section.

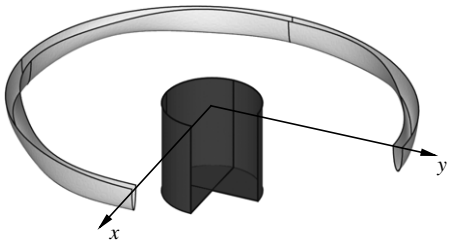

Fig. 8. Perspective view of the non-axisymmetric structure with elliptical cross-sections and $N = 15$ optimization parameters. In this case there are 5 Fourier modes in the azimuthal direction. One quadrant is omitted for clarity.

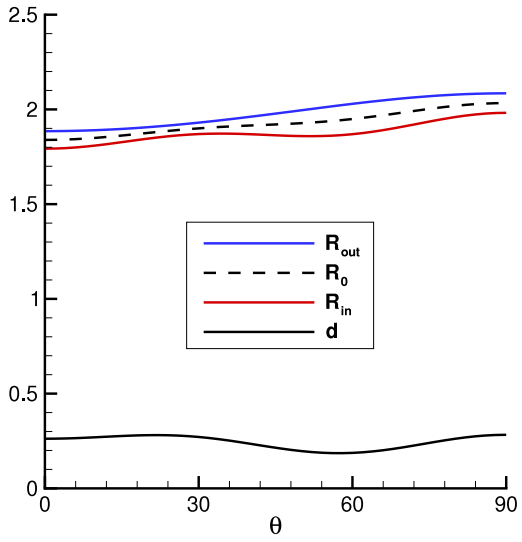

Fig. 9. Azimuthal variation of the radii of the outer and inner waterlines and depth d for the non-axisymmetric ring shown in Fig. 8. The dashed line is the radius of the axis.

5. Continuous rings

In this section we consider structures where the inner cylinder is surrounded by a continuous ring. The simplest example is a torus with semi-elliptical cross-sections defined by

$$R = R_0 + b \sin \psi, \tag{12}$$

$$z = -d \cos \psi. \tag{13}$$

Here (R, z) are cylindrical coordinates with R being the radius from the vertical z-axis. The parametric coordinate ψ varies between $-\pi/2$ on the inner waterline and $\pi/2$ on the outer waterline, with $\psi = 0$ at the deepest point of the section. The three optimization parameters include the radius R_0 of the toroidal axis, the horizontal semi-axis (half-beam) b, and the vertical semi-axis (depth) d.

More general rings are defined using Fourier series to represent both the dependence on the parametric coordinate ψ, and the azimuthal variation depending on θ:

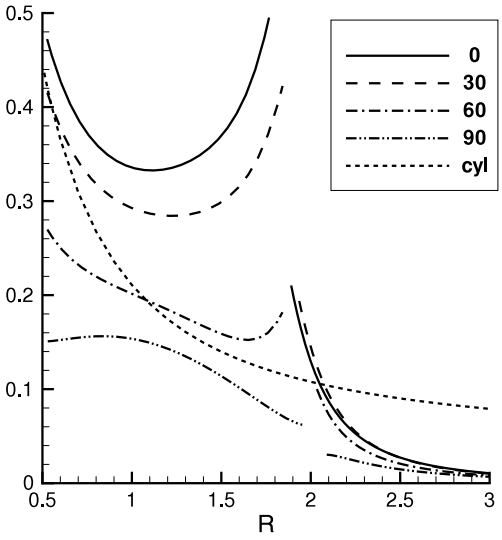

Fig. 10. Amplitude of the free-surface elevation for the structure shown in Fig. 8 at $\theta = (0, 30, 60, 90)$ degrees from the x-axis, normalized by the amplitude A of the incident waves. The gaps in the curves correspond to the segments of the free surface between the inner and outer radii of the ring, as shown in Fig. 9. The continuous dashed line is the amplitude for the uncloaked cylinder, at $\theta = 0$.

$$R = \sum_{i=1}^{I} R_i \cos 2(i-1)\theta + \sum_{i=1}^{I} \left[\sum_{j=1}^{J_s} S_{ij} \sin j\psi + \sum_{j=1}^{J_c} C_{ij} \cos j\psi \right] \cos 2(i-1)\theta, \tag{14}$$

$$z = -\left(\sum_{i=1}^{I} d_i \cos 2(i-1)\theta \right) \cos \psi. \tag{15}$$

The number of optimization parameters $(R_i, S_{ij}, C_{ij}, d_i)$ is $N = I \times (J_s + J_c + 2)$. Two specific cases will be considered: (a) axisymmetric rings $(I = 1)$ with $(J_s = J_c)$ and $(N = 4, 6, 8, 10, 12, 14, 16)$, and (b) non-axisymmetric rings with elliptical sections where $(J_s = 1, J_c = 0)$ and $(N = 3I = 3, 6, 9, 12, 15)$. Optimized values of the energy ratio are shown for both cases in Fig. 6.

Fig. 7 shows the cross-sections of the axisymmetric rings. For $(N > 3)$ these have a substantial inclination, radially inward for increasing depth, compared to the vertical axis of the semi-ellipse $(N = 3)$. The sections are rather extreme for $(N > 4)$ and give relatively small reductions of the energy. The smallest value $E/E_0 = 1.7 \times 10^{-6}$ is achieved with $N = 16$.

The energy ratios of the non-axisymmetric rings are substantially smaller, as shown in Fig. 6. The smallest value $E/E_0 = 5.2 \times 10^{-9}$, which is obtained with the maximum number of optimization parameters $(N = 15)$, is within the estimated limit of computational accuracy. This configuration is shown in Figs. 8 and 9.

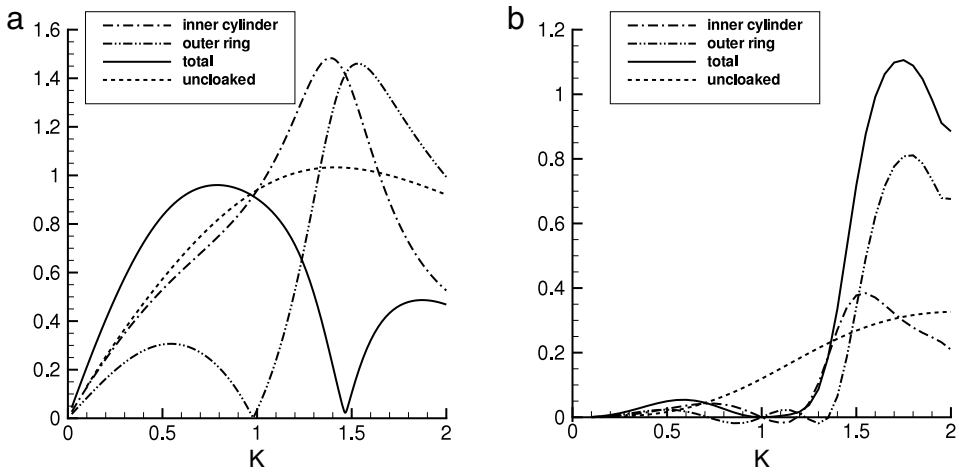

Fig. 11. Horizontal forces acting on the structure shown in Fig. 8 including the first-order exciting force (a) and second-order mean drift force (b). The dashed lines are the forces acting on the uncloaked cylinder.

Comparison of the results in Fig. 6 suggests that perfect cloaking may be possible, but only with a non-axisymmetric ring. Notwithstanding this hypothesis, surprisingly small values of the scattered energy can be achieved with axisymmetric structures.

Fig. 10 shows the amplitude of the scattered waves for the structure in Fig. 8, at $K = 1$. The waves between the cylinder and the surrounding ring are relatively large. Outside the ring they decay rapidly with increasing radius, relative to the uncloaked cylinder. Since the real part of the potential is symmetric about $x = 0$ and the imaginary part is anti-symmetric, the amplitude of the scattered waves is the same in all four quadrants.

The first-order exciting force is shown in Fig. 11(a). The separate components acting on the inner cylinder and outer ring are shown as well as the total force on the complete structure. By comparison with the uncloaked cylinder, the total force is increased for long wavelengths ($K < 1$) and decreased substantially for shorter waves. The separate components are relatively large but with opposite phases, and the total force is close to zero near $K = 1.47$. For $K < 1$ the force on the inner cylinder is practically the same as for the uncloaked case. At $K = 0.98$ the force on the outer ring is close to zero.

The drift force in Fig. 11(b) is similar to the scattered energy, as expected, with very small values near $K = 1$. It is interesting to note that the separate components have simple zeros close to this point, crossing in opposite directions. Since the symmetric and anti-symmetric components of the potential are respectively real and imaginary, there is no anti-symmetric component of the second-order mean pressure and no drift force acting on symmetrical sub-elements of the body. The total drift force is positive (or zero); within the accuracy of the plot it appears to have a second-order zero.

6. Conclusions

Examples of broadband cloaking have been demonstrated for a circular cylinder in deep water. Two types of surrounding structures are used, an array of smaller cylinders and a continuous ring. In both cases the total scattered energy is reduced substantially for wavenumbers near $K = 1$. This may have practical applications, particularly to reduce the mean drift force on offshore structures.

The most interesting question from the scientific standpoint is whether perfect cloaking can be achieved. It is generally assumed that diffraction by a fixed structure involves non-zero scattered waves which propagate outward in the far field. This phenomenon is intuitively obvious. The possibility that structures exist for which there are no scattered waves, even at one wavenumber, may be considered surprising if not impossible.

The present work is based on a program with greater accuracy than is generally required for normal engineering analysis. The standard version of the radiation–diffraction code WAMIT, which was used for the earlier work reported in [5], has a maximum accuracy of 4 or 5 decimals. This was not sufficient to show significant differences in the minimum scattered energy of axisymmetric and non-axisymmetric structures. The extended program used here is considered to have an absolute accuracy for the present results on the order of 9 or 10 decimals. The comparison in Fig. 6 shows a substantial reduction in the minimum scattered energy for structures which vary in the azimuthal direction and suggests that perfect cloaking can only be achieved with non-axisymmetric structures.

The minimum computed value of the scattered energy for the cylinder arrays in Section 4 is $E = 1.1 \times 10^{-9}$. The minimum value for the continuous rings in Section 5 is $E = 3.8 \times 10^{-10}$. These are evidently at or near the limits of the computational accuracy and cannot be distinguished from perfect cloaking. They provide tentative numerical evidence for the existence of perfect cloaking. The establishment of a rigorous analytic proof to support (or refute) this statement is a challenging goal for future research.

References

[1] R. Porter, Cloaking of a cylinder in waves, in: 26th International Workshop on Water Waves and Floating Bodies, Athens, 2011. http://www.iwwwfb.org/Abstracts/iwwwfb26/iwwwfb26_36.pdf.

[2] J.N. Newman, Scattering by a cylinder with variable bathymetry, in: 27th International Workshop on Water Waves and Floating Bodies, Copenhagen, 2012. http://www.iwwwfb.org/Abstracts/iwwwfb27/iwwwfb27_33.pdf.

[3] R. Porter, J.N. Newman, Cloaking of a vertical cylinder in waves using variable bathymetry, submitted for publication.

[4] M. Farhat, S. Enoch, S. Guenneau, A.B. Movchan, Broadband cylindrical acoustic cloak for linear surface waves in a fluid, Phys. Rev. Lett. 101 (2008) 134501.

[5] J.N. Newman, Cloaking a circular cylinder in deep water, in: 28th International Workshop on Water Waves and Floating Bodies, L'Isle sur la Sorgue, France, 2013. http://www.iwwwfb.org/Abstracts/iwwwfb28/iwwwfb28_40.pdf.

[6] J.N. Newman, The interaction of stationary vessels with regular waves, in: 11th Symposium on Naval Hydrodynamics, London, 1976, pp. 491–501.

[7] Anon., WAMIT User Manual, Version 7.0, WAMIT, Inc., Chestnut Hill, MA, USA, 2013. http://www.wamit.com/manual.htm.

[8] http://people.sc.fsu.edu/~jburkardt/f_src/praxis/praxis.html.

[9] C.-H. Lee, J.N. Newman, Computation of wave effects using the panel method, in: S. Chakrabarti (Ed.), Numerical Models in Fluid—Structure Interaction, WIT Press, Southampton, 2004.

[10] J.N. Newman, Algorithms for the free-surface Green function, J. Engrg. Math. 19 (1985) 57–67.